Desalination and Water Treatment
www.deswater.com
1944-3994/1944-3986 © 2013 Desalination Publications. All rights reserved
doi: 10.1080/19443994.2012.704718

51 (2013) 1229–1241
January

Taylor & Francis
Taylor & Francis Group

Parametric equations for the variables of a steady-state model of a multi-effect desalination plant

Patricia Palenzuela*, Diego Alarcón, Guillermo Zaragoza, Julián Blanco, Mercedes Ibarra

CIEMAT-Plataforma Solar de Almería, Ctra. de Senés s/n, 04200 Tabernas, Almería, Spain
Tel. +34 950387909; Fax: +34 950365015; email: patricia.palenzuela@psa.es

Received 8 April 2012; Accepted 15 June 2012

ABSTRACT

In this work a steady-state model is developed of an MED plant. Its development and validation have been carried out by experimental data obtained from an MED pilot plant located at the Plataforma Solar de Almería (PSA), in the southeast of Spain. It is a vertical arrangement forward-feed MED plant with preheaters, which uses hot water as the thermal energy source. In order to run the model, a series of parametric equations have been determined for the following variables: the overall heat transfer coefficient for the first effect (U_h), the overall heat transfer coefficient for the preheaters ($U_p(i)$), the vapor temperature inside the first effect ($T_v(1)$), and the cooling seawater outlet temperature (T_{cwout}). They have been obtained from a three-level factorial experimental design (3^k), performing a total of 81 experiments (3^4). The results obtained showed a good fit to the estimated models for the response variables.

Keywords: Solar desalination; Multi-effect distillation; Modeling

1. Introduction

Industrial desalination of seawater is one of the possible solutions to alleviate the worldwide scarcity of freshwater. The industrial desalination processes can be split into two main categories: (1) thermal processes that include multi-stage flash (MSF) and multi-effect distillation (MED) as the most commercially successful and (2) membrane processes including reverse osmosis (RO). The advantages of thermal desalination processes are their ability to be driven by low energy thermal sources, their reliability, easier operation and maintenance and high purity freshwater. Among the thermal desalination processes, MED has the highest thermal efficiency and the lowest power consumption [1]. However, the disadvantage of thermal desalination processes is that the overall energy consumption is high, so the use of renewable energies is required to guarantee the sustainability of this technological option [2,3]. The usual coincidence in many locations of fresh water shortage, abundant seawater resources and high isolation levels makes thermal seawater desalination driven by solar energy as one of the most promising processes to obtain fresh water. This can be possible by the coupling of a conventional thermal distillation plant with a solar thermal system [4].

The improvement in the design of a MED process can be reached by the prediction of its performance over a wide range of operating conditions. Mathematical modeling and computer simulations can provide an insight into the workings of the system and help to

*Corresponding author.

Presented at the International Conference on Desalination for the Environment, Clean Water and Energy, European Desalination Society, 23–26 April 2012, Barcelona, Spain

understand in detail the process elements in order to predict the behavior and the efficiency of the system. Many articles have been published on the topic of modeling and simulation of MED processes. El-Dessouky et al. have made several contributions in the mathematical modeling of MED plants [5,6]. El-Nashar et al. [7,8] presented a mathematical simulation of the steady-state operation of a solar MED unit, which was validated with experimental data from a pilot plant located at Abu Dhabi, UAE. A computer simulation model of a multi-effect thermal vapor compression (TVC-MED) was presented by Kamali [9] to predict the influence of all factors on heat transfer coefficients, temperature and pressure, total capacity and performance ratio of the system under design and operating conditions. Also, Trostmann [10] developed a model and carried out steady-state simulations of a MED-TVC, where heat transfer coefficients correlations for condensation and evaporation in the tubes were discussed and compared. Gautami et al. [11] developed mathematical models in order to select the optimal configuration of a MED process based on the product concentration and steam economy. Finally, the authors developed a model of an MED plant, based on the MED pilot plant located at the Plataforma Solar de Almería (PSA) [12]. To solve this model, a parameterization of the overall heat transfer coefficients was carried out by performing a series of experiments at the MED-PSA plant. The correlations obtained were based on the characterization published by El-Nashar [8].

In this study, new correlations have been obtained by the authors by means of a parametric study. The parametric equations have been determined for the following variables: the overall heat transfer coefficient for the first effect (U_h), the overall heat transfer coefficient for the preheaters ($U_p(i)$), the vapor temperature inside the first effect ($T_v(1)$), and the cooling seawater outlet temperature ($T_{cw,out}$). Such parametric equations have been obtained using a factorial design.

2. Description of the plant

2.1. Process design

The desalination plant at the PSA, with 14 cells or effects, is a forward-feed MED unit manufactured and delivered by ENTROPIE in 1987 [13]. The cells are in a vertical arrangement at decreasing pressures from cell 1 to cell 14 [14]. The first cell, which was modified in 2005 within the framework of a project called AQUASOL, works with hot water as the heat transfer media [15]. Originally, the first cell worked with low-pressure saturated steam (70˚C, 0.31 bars). The hot water for the first cell is provided either with a solar field composed of static compound parabolic concentrators (CPC) or with a double-effect absorption heat pump, DEAHP (LiBr-H_2O), which was manufactured by ENTROPIE in 2005 in the framework of the AQUASOL project [16–18]. In the modelling developed in this study, only the case in which the hot water comes from the solar filed has been taken into account.

The flow sheet of the process is shown in Fig. 1. Firstly, the pumped feed seawater flows through the condenser and the preheaters of the plant in order to preheat it before reaching the first effect. Once in the first effect, the seawater is sprayed through a spraying

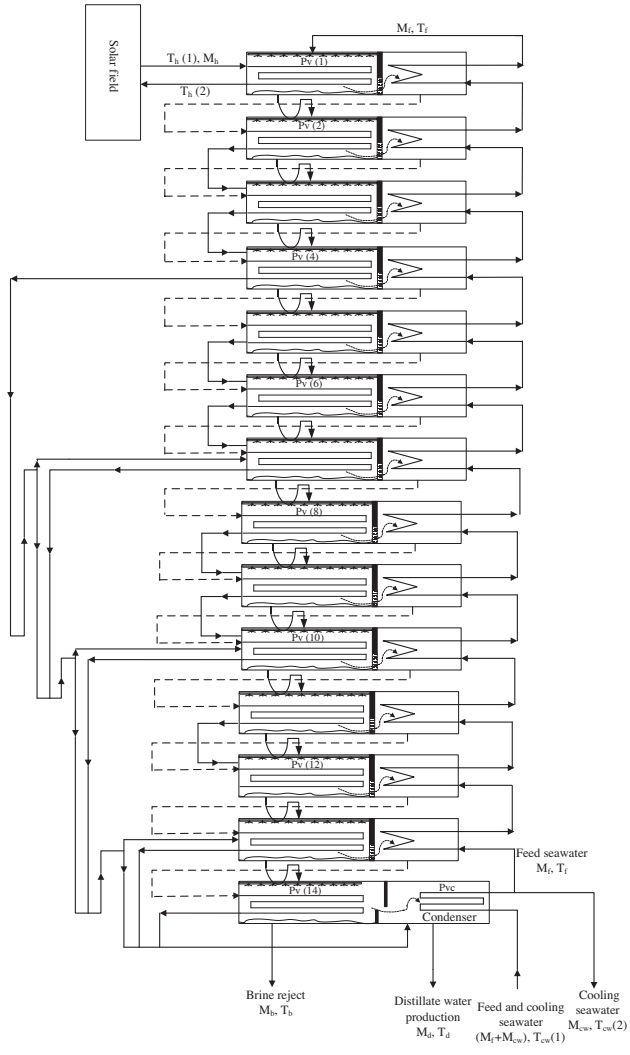

Fig. 1. Schematic diagram of the multi-effect distillation plant at the Plataforma Solar de Almería. Dashed lines show the steam flow; solid lines the distillate flow; U-shaped lines represent the brine flow from one effect to the next.

tray falling over a horizontal-tube bundle. Then, it is built on thin falling film that coats the surface of the tubes entirely. On the other hand, the hot water flows inside the tubes and releases its sensible heat to the seawater, evaporating part of it. Vapor generated in the first effect flows to the preheater located next to it, through a wire mesh demister that removes the entrained brine droplets. Here, vapor transfers part of its latent heat to the seawater which is circulating inside the preheater bundle tube, increasing its temperature. As a consequence, a small amount of the vapor condenses, which is the first distillate of the process. The vapor that has not condensed flows through the inside of the second effect tube bundle, being the thermal energy source in the evaporation–condensation process in this effect. Then, the vapor condenses by transferring its latent heat to the more concentrated brine flowing from the previous effect.

The same process is repeated in the rest of effects, being the vapor produced in the previous effect the thermal energy source of the effect. In each effect, as in the first one, part of the vapor generated is used to preheat the seawater that flows through the preheaters. Finally, the vapor produced in the last effect is led to the end condenser, where is condensed by transferring the latent heat of evaporation to the cooling seawater which is passing through the condenser bundle tube. That heated seawater is divided into two streams, some is pumped to the first effect of the plant after passing through the preheaters of each effect and the rest is rejected.

The vapor condensed in each effect and in the preheaters together with the distillate from the last condenser make up the total distillate of the plant. In order to improve the process from an energetic point of view, the distillate produced in each effect goes to other effects of the plant to recover part of its sensible heat. In some cases, the distillate goes from an effect to the next one, and in other cases, it goes to further effects as follows: in the fourth cell all the distillate is extracted, part of it goes to the seventh cell and the rest to the tenth. Similar extraction is made in the seventh cell, splitting the condensate between the tenth and the thirteenth effects. Another extraction takes place from the tenth cell, part goes to the thirteenth effect and the rest is mixed with the distillate produced in the fourteenth effect. The final extraction is made in the thirteenth effect, after which all the distillate is mixed with that produced in the fourteenth effect. Finally, this accumulated distillate is mixed with the distillate from the condenser, making up the total production.

Besides the vapor formed by boiling, a small portion is formed by flashing. When the distillate and the brine pass from one effect to another, some flashing takes place since they enter a cell that is at a lower pressure than the previous one.

The vacuum system consists of two hydro-ejectors, which are connected to effects 2, 7, and the end condenser. They are within a closed circuit with a tank and an electric pump that pumps seawater through the ejectors at a pressure of 3 bar. This vacuum system does the initial vacuum of the plant removing the air and the non-condensable gases generated during the desalination process.

The design specifications of the PSA MED plant are given in Table 1. The tube bundles of the heater, evaporators, preheater, and condenser are made of 90–10 Cu–Ni tubes. The surface areas of each of the different tube bundles are the following:

- First effect evaporator bundle, 24.26 m^2.
- Effects 2–14 evaporator bundle, 26.28 m^2.
- Preheater bundle, 5 m^2.
- Condenser bundle, 18.3 m^2.

2.2. Experimental set-up

The MED-PSA plant is experimental and therefore equipped with a comprehensive monitoring system, which provides instantaneous values of the measured data. The monitored data are detailed in Table 2 and are also indicated in Fig. 1.

The supply water to the desalination plant is obtained from wells and stored in a pool from where the cooling water is pumped to the bundle tube of the condenser. Afterwards, part of it is used as feed water

Table 1
Design specifications of the MED-PSA plant

Number of effects	14
Feed seawater flow rate	8 m^3/h
Brine flow rate from the last effect	5 m^3/h
Hot water flow rate	12.0 L/s
Total distillate output	3 m^3/h
Cooling seawater flow rate at 25 ℃	20 m^3/h
Vapor production in the last effect at 70 ℃	159 kg/h
Heat source energy consumption	200 kW
Performance ratio	>9
Vacuum system	Hydro-ejectors (seawater at 3 bar)
Inlet/Outlet hot water temperature	74.0/70.0 ℃
Brine temperature (on the first cell)	68 ℃
Feed and cooling seawater temperature at the outlet of the condenser	33 ℃

Table 2
Monitored data at PSA MED plant

Measurement	Name of variable	Magnitude
Flow rate	M_h	Heating water flow
	M_{cw}	Cooling seawater flow
	M_f	Feed seawater flow
	M_d	Product water flow
	M_b	Brine flow
Temperature	$T_{h,in}$	Heating water inlet
	$T_{h,out}$	Heating water outlet
	T_f	1st effect sprayed seawater temp.
	$T_{cw,in}$	Cooling seawater inlet temp.
	$T_{cw,out}$	Cooling seawater (rejected) outlet temp.
Pressure	$P_v(1)$, $P_v(2)$, $P_v(4)$, $P_v(6)$, $P_v(8)$, $P_v(10)$, $P_v(12)$, $P_v(14)$	1st, 2th, 4th, 6th, 8th, 10th, 12th, 14th effect vapor press.
	$P_{h,in}$	Heating water inlet pressure
	P_{vc}	Vapor pressure in the condenser
Salt concentration	X_f	Seawater TDS at the condenser inlet

in the first effect and the rest is rejected back to the pool. Therefore, part of the heat released at the condenser goes into the pool and the cooling water temperature could increase during the experiment, which is not desirable. To avoid that, a dry cooler is switched on since the beginning of the experiment cooling the pool.

As the model proposed is at steady-state, time averages of the measured data are carried out in order to perform the modeling.

3. Mathematical model

The model is based on the steady-state mass and energy balances, and the heat transfer equations for all the components of the plant, considering the work developed by El-Dessouky and Ettouney (2002). As opposed of the model of El-Dessouky, the first effect has been modeled taking into account that this unit uses hot water as the thermal energy source instead of vapor. The model has been implemented in MATLAB environment accounting for the processes and features of the MED-PSA plant. The following assumptions have been taken into account in order to simplify the analysis: steady-state operation, negligible heat losses to the surroundings, equal temperature difference across the effects, equal temperature difference across the preheaters, salt-free distillate from all the effects, the condensate that leaves each effect is considered as saturated liquid.

To develop the model, the MED system has been divided into three blocks: the first effect, the effects 2 to N, and the end condenser. Within the second block, there are three sub-blocks: the first one, which consider the effects in which the distillate that enters comes from the previous effect and preheater (effects 3, 4, 6, 9, and 12), the effects in which the distillate that enters comes from the previous effect, from the previous preheater and from further effects (effects 7, 10, and 13), and the effects in which the distillate that enters comes from the previous preheater (effects 2, 5, 8, 11, and 14). The first two blocks (the first effect and the effects 2 to N) have two control volumes: the evaporator and the preheater. The evaporator is the part of the effect where the seawater is sprayed over the bundle tube and part of the brine is evaporated.

3.1. The first effect

Fig. 2 shows a schematic diagram of the heater, which corresponds to the first effect of the plant.

The mass, salt, and energy balances of the evaporator are the following:

- Energy balance:

$$M_h \cdot h_{h,in} + M_f \cdot h_f = m_{ev}(1) \cdot h_{ev}(1) + M_h \cdot h_{h,out} + m_b(1) \cdot h_b(1) \quad (1)$$

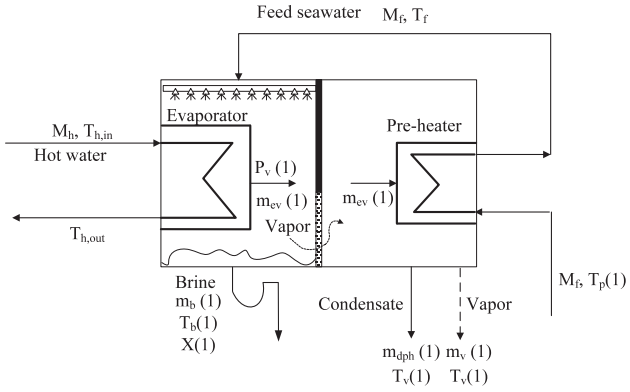

Fig. 2. Flow diagram of the heater (effect 1).

where M_h is heating water mass flow rate from the solar field, M_f is the feed seawater mass flow rate, $m_{ev}(1)$ the vapor mass flow rate that leaves the evaporator, $m_b(1)$ the brine mass flow rate that leaves the first effect, and h is the enthalpy corresponding to each stream.

- Mass and salt balances:

$$M_f = m_b(1) + m_{ev}(1) \tag{2}$$

$$X_f M_f = X(1) \cdot m_b(1) \tag{3}$$

where X_f is the feed seawater salinity and $X(1)$ the salinity of the brine that leaves the first effect.

The mass and energy balances of the preheater are the following:

- Energy balance:

$$m_{ev}(1) \cdot h_{ev}(1) + M_f \cdot h_p(1) = m_v(1) \cdot h_v(1) + m_{dph}(1) \cdot h_{dph}(1) + M_f \cdot h_f \tag{4}$$

- Mass balance:

$$m_{ev}(1) = m_v(1) + m_{dph}(1) \tag{5}$$

where $m_v(1)$ is the vapor mass flow rate that leaves the first preheater and $m_{dph}(1)$ is the distillate mass flow rate that is generated in the preheater.

It is considered that the condensate generated in the preheater and the rest of vapor leave the preheater at a temperature of $T_v(1)$ (it corresponds to the saturation pressure $P_v(1)$). This temperature is lower that of the boiling brine temperature ($T_b(1)$) by the boiling point elevation (BPE). Therefore:

$$T_b(1) = T_v(1) + (\mathrm{BPE})_1 \tag{6}$$

This parameter can be determined by a correlation published by El-Dessouky [19,20], which is as follows:

$$\mathrm{BPE}(1) = A \cdot X(1) + B \cdot X(1)^2 + C \cdot X(1)^3 \tag{7}$$

$$A = 8,325 \cdot 10^{-2} + 1,883 \cdot 10^{-4} \cdot T_b(1) + 4,02 \cdot 10^{-6} \cdot T_b(1)^2$$

$$B = -7,625 \cdot 10^{-4} + 9,02 \cdot 10^{-5} \cdot T_b(1) - 5,2 \cdot 10^{-7} \cdot T_b(1)^2$$

$$C = 1,522 \cdot 10^{-4} - 3 \cdot 10^{-6} \cdot T_b(1) - 3 \cdot 10^{-8} \cdot T_b(1)^2$$

where $X(1)$ is the salt weight percentage that leaves the first effect. The above equation is valid over the following ranges: $1 \le X(1) \le 16\%$, $10 \le T_b(1) \le 180$ ℃.

The heat transfer equation for the evaporator of the first effect can be written as:

$$Q_h = A_h \cdot U_h \cdot \frac{(T_{h,in} - T_b(1)) - (T_{h,out} - T_f)}{\ln\left(\frac{T_{h,in} - T_b(1)}{T_{h,out} - T_f}\right)} \tag{8}$$

where U_h is the overall heat transfer coefficient for the heater, A_h is the first effect evaporator bundle tube, $T_{h,in}$ the heating water inlet temperature and $T_{h,out}$ the heating water outlet temperature. Q_h is the thermal power that the hot water transfers to the seawater that is sprayed over the first effect, and it is defined as follows:

$$Q_h = M_h \cdot C_{ph} \cdot (T_{h,in} - T_{h,out}) \tag{9}$$

where C_{ph} is the hot water-specific heat.

In the case of the preheater, the heat transfer equation is given by:

$$Q_p(1) = A_p \cdot U_p \cdot \frac{(T_v(1) - T_f) - (T_v(1) - T_p(1))}{\ln\left(\frac{T_v(1) - T_f}{T_v(1) - T_p(1)}\right)} \tag{10}$$

where $U_p(1)$ is the overall heat transfer coefficient of the first preheater, A_p is the preheater bundle (it is considered the same for all the preheaters), $T_p(1)$ is the seawater temperature in the inlet of the first preheater and T_f is the seawater temperature in the outlet of the last preheater. $Q_p(1)$ is the thermal power that the vapor coming from the evaporator transfer to the seawater flowing through the tubes of the preheater and it is determined by this equation:

$$Q_p(1) = M_f \cdot C_{pf} \cdot T_f - M_f \cdot C_p(1) \cdot T_p(1) \quad (11)$$

where $C_p(1)$ and C_{pf} are the seawater-specific heat at the inlet of the first preheater and at the outlet of the last one, respectively.

3.2. Effects 2 to N

As mentioned earlier, within this block there are three sub-blocks. Each sub-block is composed by three components: the flash box, the evaporator, and the preheater. The balances corresponding to the flash box and the preheater are the same for the three blocks, but those corresponding to the evaporator are slightly different. Therefore, in each sub-block, only the evaporator will be analyzed and then the flash box and the preheater will be analyzed for the three sub-blocks.

3.2.1. Effects in which the distillate that enters comes from the previous preheater

The effects corresponding to this sub-block are the following: 2, 5, 8, 11 y 14. Fig. 3 shows a schematic diagram of a typical type of this effect.

The mass, salt, and energy balances are the following:

- Energy balance:

$$\begin{aligned} &m_{dph}(i-1) \cdot h_{dph}(i-1) + m_v(i-1) \cdot h_v(i-1) \\ &\quad + m_{br}(i) \cdot h_{br}(i) \\ &\quad = m_{ev}(i) \cdot h_v(i) + m_b(i) \cdot h_b(i) + m_d(i) \cdot h_d(i) \end{aligned} \quad (12)$$

where $m_{dph}(i-1)$ is the distillate mass flow rate coming from the preheater $i-1$, $m_v(i-1)$ is the vapor mass flow rate that leaves the preheater $i-1$ and enters the evaporator i, $m_{br}(i)$ is the brine mass flow rate that is sprayed over the evaporator I bundle tube, $m_b(i)$ is the brine mass flow rate that leaves the evaporator i and $m_d(i)$ is the distillate mass flow rate that leaves the evaporator i.

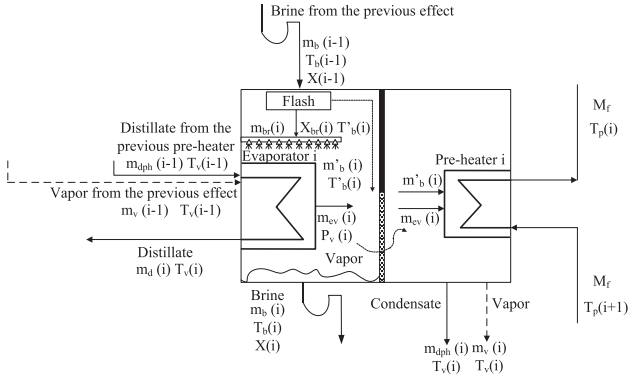

Fig. 3. Flow diagram of the effects 2, 5, 8, 11, and 14.

- Mass and salt balances:

$$m_{br}(i) = m_{ev}(i) + m_b(i) \quad (13)$$

$$m_{br}(i) \cdot X_{br}(i) = m_b(i) \cdot X(i) \quad (14)$$

where $X_{br}(i)$ is the salinity of the brine that is sprayed over the evaporator i bundle tube and $X(i)$ is the brine salinity that leaves the evaporator i.

The distillate coming from the preheater $i-1$, $m_{dph}(i-1)$, joins the condensate generated inside the tubes of the evaporator i, $m_c(i)$, which is produced from the condensation of the vapor coming from the effect $i-1$, $m_v(i-1)$. Both distillates form the total distillate in the effect i, $m_d(i)$, which leaves the effect as saturated liquid at a temperature of $T_v(i)$ (saturation temperature at the pressure $P_v(i)$):

$$m_d(i) = m_{dph}(i-1) + m_c(i) \quad (15)$$

$$m_c(i) = m_v(i-1) \quad (16)$$

3.2.2. Effects in which the distillate that enters comes from the previous effect and preheater

The effects corresponding to this sub-block are the following: 3, 4, 6, 9, and 12. Fig. 4 shows a schematic diagram of a typical type of this effect.

The mass, salt, and energy balances are the following:

- Energy balance:

$$\begin{aligned} &m_{dph}(i-1) \cdot h_{dph}(i-1) + m_d(i-1) \cdot h_d(i-1) \\ &\quad + m_v(i-1) \cdot h_v(i-1) + m_{br}(i) \cdot h_{br}(i) \\ &\quad = m_{ev}(i) \cdot h_v(i) + m_b(i) \cdot h_b(i) + m_d(i) \cdot h_d(i) \end{aligned} \quad (17)$$

- Mass and salt balances:

$$m_{br}(i) = m_{ev}(i) + m_b(i) \quad (18)$$

$$m_{br}(i) \cdot X_{br}(i) = m_b(i) \cdot X(i) \quad (19)$$

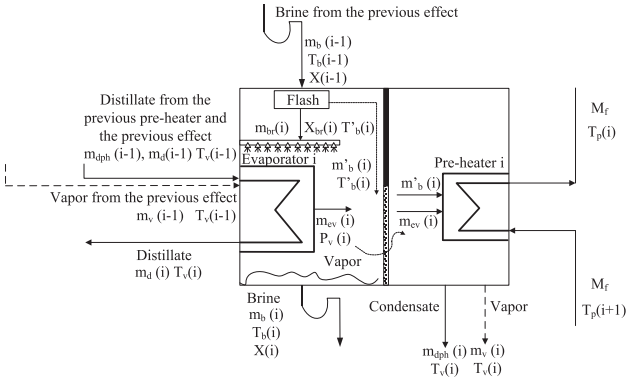

Fig. 4. Flow diagram of the effects 3, 4, 6, 9, and 12.

In this case, the distillate coming from the previous effect, $m_d(i-1)$, together with the distillate from the preheater $i-1$, $m_{dph}(i-1)$, joins the condensate generated inside the tubes of the evaporator i, $m_c(i)$. Both distillate form the total distillate in this effect, $m_d(i)$, that, as before, leaves the effect as saturated liquid at a temperature of $T_v(i)$.

$$m_d(i) = m_d(i-1) + m_{dph}(i-1) + m_c(i) \tag{20}$$

$$m_c(i) = m_v(i-1) \tag{21}$$

3.2.3. Effects in which the distillate that enters comes from the previous effect, from the previous preheater and from further effects

The effects corresponding to this sub-block are the following: 7, 10, and 13. Fig. 5 shows a schematic diagram of a typical type of this effect.

The mass, salt, and energy balances are the following:

- Energy balance:

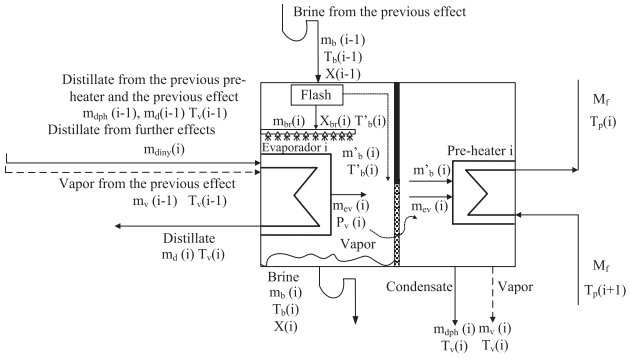

Fig. 5. Flow diagram of the effects 7, 10, and 13.

$$\begin{aligned} &m_{dph}(i-1)\cdot h_{dph}(i-1) + m_d(i-1)\cdot h_d(i-1) \\ &\quad + m_{diny}(i)\cdot h_{diny}(i) + m_v(i-1)\cdot h_v(i-1) \\ &\quad + m_{br}(i)\cdot h_{br}(i) \\ &\quad = m_{ev}(i)\cdot h_v(i) + m_b(i)\cdot h_b(i) + m_d(i)\cdot h_d(i) \end{aligned} \tag{22}$$

- Mass and salt balances:

$$m_{br}(i) = m_{ev}(i) + m_b(i) \tag{23}$$

$$m_{br}(i)\cdot X_{br}(i) = m_b(i)\cdot X(i) \tag{24}$$

In this case, the distillate coming from the previous effect, $m_d(i-1)$, together with the distillate from the preheater $i-1$ and with part of the distillate from further effects, $m_{diny}(i-1)$, joins the condensate generated inside the tubes of the evaporator i, $m_c(i)$. The three distillates form the total distillate in this effect, $m_d(i)$, that, as in the previous cases, leaves the effect as saturated liquid at a temperature of $T_v(i)$.

$$m_d(i) = m_d(i-1) + m_{dph}(i-1) + m_{diny}(i) + m_c(i) \tag{25}$$

$$m_c(i) = m_v(i-1) \tag{26}$$

The distillate mass flow rate that enters the effects 7, 10, and 13, $m_{diny}(i)$, is determined by taking into account that the sum of distillate volumetric flow rate from the previous effect and this one of the distillate that enters the effects 7, 10, and 13 is equal to $0.24\,m^3/h$. This volumetric flow rate ensures that the

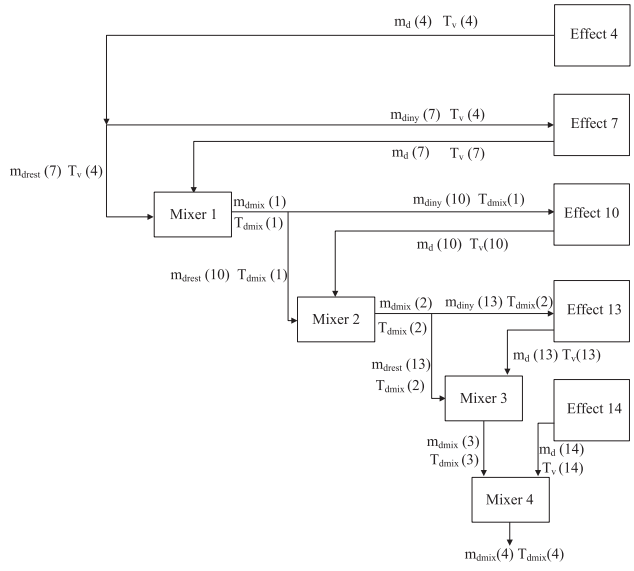

Fig. 6. Flow diagram of the extractions and injections of distillate in the effects.

rest of tubes are enough to get a suitable velocity of the vapor for the condensation process.

Fig. 6 shows a flow diagram of the inlet and outlet distillate streams between the fourth and fourteenth effects. Energy and mass balances are shown below. They will be useful to determine the distillate temperature at the outlet of the mixers and the total distillate that leaves the effects 2 to N.

The mass and energy balances through the mixers are shown below:

Mixer 1:

$$m_{\mathrm{dmix}}(1) = m_{\mathrm{drest}}(7) + m_{\mathrm{d}}(7) \tag{27}$$

$$m_{\mathrm{drest}}(7) = m_{\mathrm{d}}(4) - m_{\mathrm{diny}}(7) \tag{28}$$

$$m_{\mathrm{dmix}}(1) \cdot h_{\mathrm{dmix}}(1) = m_{\mathrm{drest}}(7) \cdot h_{\mathrm{drest}}(7) + m_{\mathrm{d}}(7) \cdot h_{\mathrm{d}}(7) \tag{29}$$

Mixer 2:

$$m_{\mathrm{dmix}}(2) = m_{\mathrm{drest}}(10) + m_{\mathrm{d}}(10) \tag{30}$$

$$m_{\mathrm{drest}}(10) = m_{\mathrm{dmix}}(1) - m_{\mathrm{diny}}(10) \tag{31}$$

$$m_{\mathrm{dmix}}(2) \cdot h_{\mathrm{dmix}}(2) = m_{\mathrm{drest}}(10) \cdot h_{\mathrm{drest}}(10) + m_{\mathrm{d}}(10) \cdot h_{\mathrm{d}}(10) \tag{32}$$

Mixer 3:

$$m_{\mathrm{dmix}}(3) = m_{\mathrm{drest}}(13) + m_{\mathrm{d}}(13) \tag{33}$$

$$m_{\mathrm{drest}}(13) = m_{\mathrm{dmix}}(2) - m_{\mathrm{diny}}(13) \tag{34}$$

$$m_{\mathrm{dmix}}(3) \cdot h_{\mathrm{dmix}}(3) = m_{\mathrm{drest}}(13) \cdot h_{\mathrm{drest}}(13) + m_{\mathrm{d}}(13) \cdot h_{\mathrm{d}}(13) \tag{35}$$

Mixer 4:

$$m_{\mathrm{dmix}}(4) = m_{\mathrm{dmix}}(3) + m_{\mathrm{d}}(14) \tag{36}$$

$$m_{\mathrm{dmix}}(4) \cdot h_{\mathrm{dmix}}(4) = m_{\mathrm{dmix}}(3) \cdot h_{\mathrm{dmix}}(3) + m_{\mathrm{d}}(14) \cdot h_{\mathrm{d}}(14) \tag{37}$$

It is considered that the distillate leaves each effect as saturated liquid at the same temperature of the vapor inside the effect, $T_{\mathrm{v}}(i)$.

As in the first effect, the temperature of the vapor generated in the effect i, $T_{\mathrm{v}}(i)$, is lower that of the boiling brine temperature in such effect ($T_{\mathrm{b}}(i)$) by the boiling point elevation (BPE)i:

$$T_{\mathrm{b}}(i) = T_{\mathrm{v}}(i) + (\mathrm{BPE})_i \tag{38}$$

The $(\mathrm{BPE})_i$ is determined by Eq. (7).

The heat transfer equation for a typical evaporator i can be written as follows:

$$Q_{\mathrm{ev}}(i) = U_{\mathrm{ev}}(i) A_{\mathrm{ev}}(i) \cdot (T_{\mathrm{v}}(i-1) - T_{\mathrm{b}}(i)) \tag{39}$$

where $U_{\mathrm{ev}}(i)$ is the overall heat transfer coefficient of a typical evaporator i, and $A_{\mathrm{ev}}(i)$ is the evaporator i bundle tube that is the same for all the evaporators from 2 to N. $Q_{\mathrm{ev}}(i)$ is the thermal power that is transferred from the vapor coming from the previous effect $(i-1)$ to the seawater sprayed over the bundle tube of the effect i. It is given by:

$$Q_{\mathrm{ev}}(i) = m_{\mathrm{v}}(i-1) \cdot \lambda_{\mathrm{v}}(i-1) \tag{40}$$

where $\lambda_{\mathrm{v}}(i-1)$ is the latent heat of formed vapor at a temperature of $T_{\mathrm{v}}(i-1)$.

In the cases of the control volumes flash and preheater, the mass and energy balances are the same for the three sub-blocks, and they are shown below.

Flash:

The brine coming from the previous effect, $m_{\mathrm{b}}(i-1)$, enters the effect i which is at a lower pressure and a portion of vapor is formed by flashing, decreasing its temperature from $T_{\mathrm{b}}(i-1)$ to $T'_{\mathrm{b}}(i)$. This temperature is higher than the boiling temperature within the effect i, $T_{\mathrm{b}}(i)$ by the non-equilibrium allowance, which is a measure of the flashing process [5]:

$$T'_{\mathrm{b}}(i) = T_{\mathrm{b}}(i) + (\mathrm{NEA})_i \tag{41}$$

This parameter can be determined by the following correlation [20]:

$$(\mathrm{NEA})_i = 33(\Delta T_{\mathrm{b}}(i))^{0.55}/T_{\mathrm{v}}(i) \tag{42}$$

where $\Delta T_{\mathrm{b}}(i)$ is:

$$\Delta T_{\mathrm{b}}(i) = T_{\mathrm{b}}(i-1) - T_{\mathrm{b}}(i) \tag{43}$$

From the flashing evaporation, an amount of vapor is obtained, $m'_{\mathrm{b}}(i)$, that joins in the way to the preheater the vapor generated by boiling, $m_{\mathrm{ev}}(i)$. The rest non-evaporated brine, $m_{\mathrm{br}}(i)$, is sprayed over the evaporator bundle tube. The energy, mass, and salts balances are shown below.

- Energy balance:

$$m_{\mathrm{b}}(i-1) \cdot h_{\mathrm{b}}(i-1) = m_{\mathrm{br}}(i) \cdot h_{\mathrm{br}}(i) + m'_{\mathrm{b}}(i) \cdot h'_{\mathrm{b}}(i) \tag{44}$$

- Mass and salts balances:

$$m_b(i-1) = m_{br}(i) + m'_b(i) \quad (45)$$

$$m_b(i-1) \cdot X(i-1) = m_{br}(i) \cdot X_{br}(i) \quad (46)$$

Preheater:

The energy and mass balances are shown below.

- Energy balance:

$$m_{ev}(i) \cdot h_{ev}(i) + m'_b(i) \cdot h'_b(i) + M_f \cdot h_p(i+1) = m_v(i) \cdot h_v(i) + m_{dph}(i) \cdot h_{dph}(i) + M_f \cdot h_p(i) \quad (47)$$

In the case of the last preheater ($i = N-1$), the seawater inlet temperature is the seawater outlet temperature from the condenser, $T_{cw,out}$, so the energy balance can be written as follows:

$$m_{ev}(N-1) \cdot h_{ev}(N-1) + m'_b(N-1) \cdot h'_b(N-1) + M_f \cdot h_{cw,out} = m_v(N-1) \cdot h_v(N-1) + m_{dph}(N-1) \cdot h_{dph}(N-1) + M_f \cdot h_p(N-1)$$

- Mass balance:

$$m_{ev}(i) + m'_b(i) = m_v(i) + m_{dph}(i) \quad (49)$$

The heat transfer equation for a typical preheater i is written as follows:

$$Q_p(i) = A_p(i) \cdot U_p(i) \cdot \frac{(T_v(i) - T_p(i)) - (T_v(i) - T_p(i+1))}{\ln\left(\frac{T_v(i) - T_p(i)}{T_v(i) - T_p(i+1)}\right)} \quad (50)$$

where $U_p(i)$ is the overall heat transfer coefficient for a typical preheater, $A_p(i)$ is the preheater bundle of a preheater (it is the same for all the preheaters), and $Q_p(i)$ is the thermal power that is transferred from the vapor coming from the evaporator i to the seawater flowing through the preheater bundle tube. It is determined as follows:

$$Q_p(i) = M_f \cdot (h_p(i) - h_p(i+1)) \quad (51)$$

In the case of the last preheater, the heat transfer equation is given by:

$$Q_p(N-1) = A_p(N-1) \cdot U_p(N-1) \cdot \frac{(T_v(N-1) - T_p(N-1)) - (T_v(N-1) - T_{cw,out})}{\ln\left(\frac{T_v(N-1) - T_p(N-1)}{T_v(N-1) - T_{cw,out}}\right)} \quad (52)$$

where $Q_p(N-1)$ is written as follows:

$$Q_p(N-1) = M_f \cdot (h_p(N-1) - h_{cw,out}) \quad (53)$$

The temperature difference across the effects (ΔT_v) and the preheaters (ΔT_p) is calculated by the following expressions:

Evaporators:

$$\Delta T_v = \frac{T_v(1) - T_v(N)}{N-1} \quad (54)$$

Then, the vapor temperature in each evaporator, $T_v(i)$, is determined as follows:

$$T_v(i) = T_v(i-1) - \Delta T_v \quad (55)$$

Preheaters:

$$\Delta T_p = \frac{T_f - T_{cw,out}}{N-1} \quad (56)$$

Therefore, the seawater temperature in each preheater is determined as follows:

$$T_p(i) = T_p(i+1) + \Delta T_p \quad (57)$$

3.3. The end condenser

The end condenser (see the flow diagram in Fig. 7) is located next to the last effect of the plant ($i = N$), so the vapor generated in this effect flows to the condenser through the demister and releases its latent heat to the seawater flowing through the bundle tube. Therefore, the vapor condenses and the seawater increases its temperature.

The mass, salt, and energy balances are the following:

- Energy balance:

$$m'_b(N) \cdot h'_b(N) + m_{ev}(N) \cdot h_{ev}(N) + (M_f + M_{cw}) \cdot h_{cw,in} = (M_f + M_{cw}) \cdot h_{cw,out} + m_{dc} \cdot h_{vc} \quad (58)$$

where M_{cw} is the cooling seawater mass flow rate.

Since negligible heat losses to the surroundings have been considered, the vapor temperature inside the effect N, $T_v(N)$, is set to be the same as the vapor temperature in the condenser, T_{vc} (it corresponds to the saturation pressure, P_{vc}).

- Mass balance:

$$m_{dc} = m_{ev}(N) + m'_b(N) \quad (59)$$

Finally, the product water of the plant, M_d, and its temperature, T_d, are determined by a mass and energy balance in the Mixer 5:

- Mass balance:

$$M_d = m_{dc} + m_{dmix}(4) \tag{60}$$

- Energy balance:

$$m_{dmix}(4) \cdot h_{dmix}(4) + m_{dc} \cdot h_{dc} = M_d \cdot h_d \tag{61}$$

On the other hand, the heat transfer equation of the end condenser is given by:

$$Q_c = A_c \cdot U_c \cdot \frac{(T_v(N) - T_{cw,out}) - (T_v(N) - T_{cw,in})}{\ln\left(\frac{T_v(N)-T_{cw,out}}{T_v(N)-T_{cw,in}}\right)} \tag{62}$$

where U_c is the overall heat transfer coefficient of the condenser, A_c is the condenser bundle, and Q_c is the thermal power transferred from the vapor coming from the last effect to the feed and cooling seawater flowing through the condenser bundle tube. It is written as follows:

$$Q_c = (M_f + M_{cw}) \cdot (h_{cw,out} - h_{cw,in}) \tag{63}$$

The model described earlier is useful to determine the performance ratio (*PR*) of the plant, which is defined as kg of distillate produced for every 2,326 kJ of thermal energy supplied to the system. Therefore, the equation to assess it is as follows:

$$PR = \frac{M_d}{Q_h} \times \frac{2326\ \text{kJ}}{1\ \text{kg}} \tag{64}$$

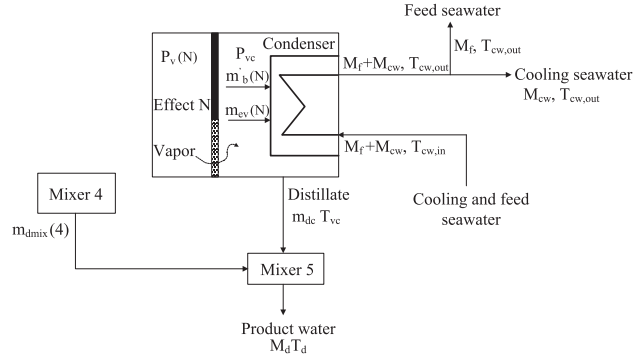

Fig. 7. Flow diagram of the end condenser.

4. Parameterization

In the equations described earlier, the following are the series of variables: the overall heat transfer coefficient for the first effect (U_h), the overall heat transfer coefficient for the preheaters ($U_p(i)$), the vapor temperature inside the first effect ($T_v(1)$), and the cooling seawater outlet temperature ($T_{cw,out}$), whose value is needed to determine in order to run the model. For this purpose, a series of parametric equations that represent these variables have been obtained from a three-level factorial experimental design (3^k), The variables or factors (k) with the actual levels of operation (low (−1), medium (0), and high (+1)) are shown in Table 3. Therefore, an experimental campaign have been performed with a total of 81 (3^4) experiments.

The experiments were carried out in 10 months, from March to January, and they were designed taking into account that the last effect vapor temperature has to be higher that the minimum seawater temperature in the Mediterranean Sea (that is 15°C) plus a temperature difference of 10°C in the condenser in order to satisfy the cooling flow rates required.

The overall heat transfer coefficient for the first effect is obtained from Eq. (8). However, for the preheaters an overall heat transfer coefficient, $\bar{U}_p$ is calculated by considering the total heat transfer, Q_p in all $N-1$ preheaters:

$$\bar{U}_p = \frac{Q_p}{A_p \cdot \Delta T_p \cdot (N-1)} \tag{65}$$

The total heat transfer rate in the $N-1$ preheaters is assessed as follows:

$$Q_p = M_f \cdot (h_f - h_{cw,out}) \tag{66}$$

A second-order response surface model (Response Surface Methodology, RSM) has been used in order to obtain the parametric equations. Each response has been linked to the factors by a second-order polynomial model with interactions as shown in the following equation [21]:

$$Y = \beta_o + \sum_{i=1}^{k} \beta_i X_i + \sum_{i=1}^{k} \beta_{ii} X_i^2 + \sum_{i=1}^{k-1} \sum_{j=2j>i} \beta_{ij} X_i X_j + \varepsilon \tag{67}$$

where Y is the response, $\beta_o, \beta_1, \ldots, \beta_k$, β_{ij} are the regression coefficients, X_i, X_j $(j = i+1, \ldots, k)$ represent the independent variables or factors (last effect vapor temperature, $T_v(14)$, heating water inlet temperature, $T_{h,in}$, feed seawater flow, M_f, and heating water flow, M_h) and ε is the statistical error.

Table 3
Variable factors and their actual values of operation

	Symbol	−1	0	+1
Last effect vapor temperature (℃)	$T_v(14)$	25	30	35
Heating water inlet temperature (℃)	$T_{h,in}$	65	70	75
Feed seawater flow (m^3/h)	M_f	6	7	8
Heating water flow (L/h)	M_h	7	9.5	12

The RSM model coefficients for each response are computed by multiple linear regression (MLR) method ([21,22]):

$$\beta = (X^T X)^{-1} X^T Y \tag{68}$$

where β is the vector formed by the regression coefficients, X is the matrix ($N \times u$) of the independent variables, u is the number of regression coefficients in the RS-model (Eq. (67)) and Y is a vector ($N \times 1$) formed by the responses of the N experiments. According to this method, the β coefficients are determined by the method of least squares. In other words, the β values are chosen in order to minimize the sum of squared residuals.

For each response variable, the parametric equations with the corresponding regression coefficients have been determined.

5. Results and discussion

The independent and dependent variables are fitted to the second-order model equation (Eq. (67)) and for each response variable is examined the goodness of fit. It and the significance of each regression coefficient were obtained using the *Modde 5.0* software with a confidence level of 95%. Tables 4 and 5 present the regression relationships for each response monitored and the p values. They are used as a tool to check the significance of each of the coefficients, which in turn may indicate the pattern of the interaction between the variables. The smaller the value of p, the more significant is the corresponding coefficient [23].

The following regression equations represent the best description of the variables $T_v(1)$, $T_{cw,out}$, U_h and U_p after the elimination of non-significant parameters ($p > 0.05$) from the results summarized in Tables 4 and 5:

$$\begin{aligned} T_v(1) = {} & 85.9763 - (1.06873 \cdot T_v(N)) - (1.20385 \\ & \cdot T_{h,in}) - (0.974267 \cdot M_f) + (1.43293 \cdot M_h) \\ & + (0.0104179 \cdot T_{h,in}^2) - (0.055331 \cdot M_h^2) \\ & + (0.017083 \cdot T_v(N) \cdot T_{h,in}) \end{aligned} \tag{69}$$

$$\begin{aligned} T_{cw,out} = {} & -19.8783 + (1.27265 \cdot T_v(N)) \\ & + (0.432938 \cdot T_{h,in}) - (0.193712 \cdot M_h) \\ & + 0.00391375 \cdot T_v^2(N)) - (0.00199305 \\ & \cdot T_{h,in}^2) + (0.00936997 \cdot M_h^2) - (0.00632534 \\ & \cdot T_v(N) \cdot T_{h,in}) \end{aligned} \tag{70}$$

$$\begin{aligned} U_h = {} & 25.1217 - (0.0992825 \cdot T_v(N)) - (0.678212 \\ & \cdot T_{h,in}) + (0.30056 \cdot M_h) - (0.00323972 \\ & \cdot T_v^2(N)) + (0.00392379 \cdot T_{h,in}^2) - (0.0112135 \\ & \cdot M_h^2) + (0.00442078 \cdot T_v(N) \cdot T_{h,in}) \end{aligned} \tag{71}$$

$$U_p = -0.000540399 + (0.836569 \cdot M_f) \tag{72}$$

The goodness of fit of the model is evaluated by the coefficient of determination (R^2). It is defined as the proportion of variation in the response attributed to the model. It is suggested that R^2 should be closed to 1 for a good fit model [24]. However, a large value of R^2 does not always imply that the regression model is a good one. R^2 always increases with the addition of a new variable to the model, regardless of weather additional variable is statistically significant or not [25]. Thus, it is preferred to use the adjusted-R^2 to evaluate the model adequacy since it is adjusted for the number of terms in the model. The adjusted-R^2 should be over 90% indicating a high degree of correlation between the observed and predicted values [25]. Besides these coefficients, another one to evaluate the goodness of fit of the model is the coefficient Q^2, which is defined as the fraction of variation of the response that can be predicted by the model. Values of Q^2 close to 1 indicate a very good model [26]. Table 6 summarizes the statistics used to test the adequacy of the model. The results indicate that all the fit

Table 4
Test of significance for the response variable $T_v(1)$ and $T_{cw,out}$ regression coefficients

Model term	T_v (1)		$T_{cw,out}$	
	Coefficient estimate	p-Value	Coefficient estimate	p-Value
$T_v(N)$	−0.460	<0.05	1.308	<0.05
T_{hin}	−1.295	<0.05	0.470	<0.05
M_f	7.725	<0.05	0.172	0.1273
M_h	0.798	<0.05	−0.051	<0.05
$T_v(N) \cdot T_v(N)$	−0.005	0.2022	0.004	<0.05
$T_{hin} \cdot T_{hin}$	0.011	<0.05	−0.002	<0.05
$M_f \cdot M_f$	0.679	0.5778	0.212	0.4544
$M_h \cdot M_h$	0.052	<0.05	0.009	<0.05
$T_v(N) \cdot T_{hin}$	0.015	<0.05	−0.006	<0.05
$T_v(N) \cdot M_f$	−0.056	0.2694	−0.021	0.0,720
$T_v(N) \cdot M_h$	−0.009	0.1212	$3.517 \cdot 10^{-3}$	0.8013
$T_{hin} \cdot M_f$	−0.060	0.2,508	−0.003	0.7984
$T_{hin} \cdot M_h$	0.013	<0.05	−0.001	0.3075
$M_f \cdot M_h$	−0.013	0.8967	−0.024	0.3117

Table 5
Test of significance for the response variable U_h and U_p regression coefficients

Model term	U_h		U_p	
	Coefficient estimate	p-Value	Coefficient estimate	p-Value
$T_v(N)$	−0.478	<0.05	$-8.114 \cdot 10^{-4}$	0.4614
T_{hin}	−1.353	<0.05	$1.824 \cdot 10^{-4}$	0.2099
M_f	1.000	0.4903	0.838	<0.05
M_h	0.463	<0.05	$-7.177 \cdot 10^{-4}$	0.9957
$T_v(N) \cdot T_v(N)$	−0.001	0.2106	$1.205 \cdot 10^{-5}$	0.1451
$T_{hin} \cdot T_{hin}$	0.008	<0.05	$-3.321 \cdot 10^{-6}$	0.7024
$M_f \cdot M_f$	−0.065	0.8385	$-2.121 \cdot 10^{-4}$	0.9324
$M_h \cdot M_h$	−0.008	0.1,079	$-2.769 \cdot 10^{-5}$	0.4586
$T_v(N) \cdot T_{hin}$	0.008	<0.05	$3.978 \cdot 10^{-6}$	0.5626
$T_v(N) \cdot M_f$	−0.006	0.6662	$-1.319 \cdot 10^{-4}$	0.2087
$T_v(N) \cdot M_h$	−0.002	0.3157	$5.453 \cdot 10^{-6}$	0.6590
$T_{hin} \cdot M_f$	−0.007	0.6168	$3.738 \cdot 10^{-5}$	0.7267
$T_{hin} \cdot M_h$	−0.003	0.0811	$1.321 \cdot 10^{-5}$	0.3011
$M_f \cdot M_h$	−0.006	0.8054	$7.617 \cdot 10^{-5}$	0.7119

indices show a good fit to the estimated models for all the variables ($T_v(1)$, $T_{cw,out}$, U_h and U_p).

6. Conclusions

A mathematical model of an MED plant has been developed and validated with experimental data obtained from an MED pilot plant located at the PSA. In order to run the model, a series of parametric equations have been determined using a 3^4 factorial design with a total of 81 experiments. The variable factors were varied using a wide operational range (varying the last effect vapor temperature from 25 to 35°C, the heating water inlet temperature in the range of 65–75 °C, the feed water flow from 6 to 8 m^3/h and the heating water flow in the range of 7–10 L/s). The developed model equations can be used to predict the overall heat transfer coefficient for the first effect (U_h), the overall heat transfer coefficient for the preheaters ($U_p(i)$), the vapor temperature inside the first effect ($T_v(1)$), and the cooling seawater outlet temperature ($T_{cw,out}$), as influenced by operating factors studied in

Table 6
Statistics used to test goodness of fit of the models

	$T_v(1)$	$T_{cw,out}$	U_h	U_p
R^2	0.984	0.999	0.940	0.999
Adjusted-R^2	0.983	0.999	0.934	0.999
Q^2	0.980	0.998	0.924	0.998

this system. The results showed a good agreement between the predicted and experimental data for all the variables, with a R^2, adjusted-R^2, and Q^2 higher than 90%.

References

[1] X. Wang et al., Low grade heat driven multi-effect distillation technology, Int. J. Heat Mass Transfer 54 (2011) 5497–5503.
[2] E. Mathioulakis, V. Belessiotis, E. Delyannis, Desalination by using alternative energy: Review and state-of-the-art, Desalination 203 (2007) 346–365.
[3] G. Lourdes, Renewable energy applications in desalination: State of the art, Solar Energy 75 (2003) 381–393.
[4] L. García-Rodríguez, Seawater desalination driven by renewable energies: A review, Desalination 143 (2002) 103–113.
[5] H. El-Dessouky, I. Alaitiqi, S. Bingulac, H. Ettouney, Steady-state analysis of the multiple effect evaporation desalination process, Chem. Eng. Technol. 21 (1998) 437–451.
[6] H.T. El-Dessouky, H.M. Ettouney, Multiple-effect evaporation desalination systems. thermal analysis, Desalination 125 (1999) 259–276.
[7] A.M. El-Nashar, A.A. Qamhiyeh, Simulation of the steady-state operation of a multi-effect stack seawater distillation plant, Desalination 101 (1995) 231–243.
[8] A.M. El-Nashar, Predicting part load performance of small MED evaporators—A simple simulation program and its experimental verification, Desalination 130 (2000) 217–234.
[9] R.K. Kamali, A. Abbassi, S.A. Sadough Vanini, A simulation model and parametric study of MED–TVC process, Desalination 235 (2009) 340–351.
[10] A. Trostmann, Improved approach to steady state simulation of multi-effect distillation plants 7 (2009) 93–110.
[11] G. Gautami, S. Khanam, Selection of optimum configuration for multiple effect evaporator system, Desalination 288 (2012) 16–23.
[12] P. Palenzuela et al., Modeling of the heat transfer of a solar multi-effect distillation plant at the Plataforma Solar de Almería, Desalin. Water Treat. 31 (2011) 257–268.
[13] E. Zarza (Ed.), Solar Thermal Desalination Project, First Phase Results and Second Phase Description, CIEMAT, Madrid, Spain, 1991.
[14] E. Zarza, Solar Thermal Desalination Project Phase II Results & Final Project, Report, 1994.
[15] D. Alarcón-Padilla, L. García-Rodríguez, Application of absorption heat pumps to multi-effect distillation: A case study of solar desalination, Desalination 212 (2007) 294–302.
[16] D. Alarcón-Padilla, L. García-Rodríguez, J. Blanco-Gálvez, Assessment of an absorption heat pump coupled to a multi-effect distillation unit within AQUASOL project, Desalination 212 (2007) 303–310.
[17] D. Alarcón-Padilla et al., First experimental results of a new hybrid solar/gas multi-effect distillation system: The AQUA-SOL project, Desalination 220 (2008) 619–625.
[18] D.C. Alarcón-Padilla, L. García-Rodríguez, J. Blanco-Gálvez, Experimental assessment of connection of an absorption heat pump to a multi-effect distillation unit, Desalination 250 (2010) 500–505.
[19] H. El-Dessouky, H. Ettouney, I. Alatiqi, G. Al-Nuwaibit, Evaluation of steam jet ejectors, Chem. Eng. Process 41 (2002) 551–561.
[20] H. El-Dessouky, H. Ettouney (Eds.), Fundamentals of Salt Water Desalination, Elsevier Science BV, Amsterdam, 2002.
[21] M. Khayet et al., Optimization of solar-powered reverse osmosis desalination pilot plant using response surface methodology, Desalination 261 (2010) 284–292.
[22] D.C. Montgomery, R.H. Myers (Eds.), Response surface methodology: Process and product in optimization using designed experiments, John Wiley & Sons, New York, 1995.
[23] A. Haber, R. Runyon (Eds.), General Statistics, 3rd ed., John Wiley & Sons., New York, 1977.
[24] F. Xiangli et al., Optimization of preparation conditions for polydimethylsiloxane (PDMS)/ceramic composite pervaporation membranes using response surface methodology, J. Membr. Sci. 311 (2008) 23–33.
[25] P. Onsekizoglu, K. Savas Bahceci, J. Acar, The use of factorial design for modeling membrane distillation, J. Membr. Sci. 349 (2010) 225–230.
[26] George E.P. Box, William G. Hunter, J. Stuart, (Eds.), Statistics for Experimenters: An Introduction to Design, Data Analysis and Model Building, Wiley, New York, NY, 1978.